

## Laboratory and Field Experimental Study of Underwater Inflatable Co-prime Sonar Array (UICSA)

Yanjun Li<sup>1</sup>, Bing Ouyang<sup>1</sup>, Tongdi Zhou<sup>2</sup>, Jordan Thomas<sup>3</sup>, Shadi Bavar<sup>4</sup>, Ethan Weber<sup>1</sup>, Lorenzo Michieletto<sup>1</sup>, Tsung-chow Su<sup>5</sup>, Fauzia Ahmad<sup>2</sup>

1. Harbor Branch Oceanographic Institute, Florida Atlantic University, Fort Pierce, FL 34946, USA

2. Department of Electrical and Computer Engineering, Temple University, Philadelphia, PA 19085, USA

3. Institute for Sensing and Embedded Network Systems Engineering, Florida Atlantic University, Boca Raton, FL 33431, USA

4. Southeast National Marine Renewable Energy Center, Florida Atlantic University, Boca Raton, FL 33431, USA

5. Department of Ocean and Mechanical Engineering, Florida Atlantic University, Boca Raton, FL 33431, USA  
E-mail: yanjunleo@gmail.com; bouyang@fau.edu; tzhou@temple.edu; jbt18@vt.edu; sbavar@umass.edu; webere@fau.edu; fau\_lmichieletto@fau.edu; su@fau.edu; fauzia.ahmad@temple.edu

Received: 22 November 2021; Accepted: 20 January 2022; Available online: 10 February 2022

---

**Abstract:** This paper discusses the design and initial testing of a novel hydrophone array system dubbed the Underwater Inflatable Co-prime Sonar Array (UICSA). The UICSA will be a crucial component of an underwater deployable sensing network that can be rapidly deployed using compact autonomous underwater vehicles (AUVs). The UICSA initially is packed in a compact container to fit the payload space of an AUV. After deployment, the UICSA expands to its predetermined full length to acquire sensing data for source localization. More specifically, the mechanical compression of the UICSA is achieved through a non-rigid array support structure, which consists of flexible inflatable segments between adjoining hydrophones that are folded in order to package the UICSA for deployment. The system exploits compression in hydrophone layouts by utilizing a sparse array configuration, namely the co-prime array since it requires fewer hydrophones than a uniform linear array of the same length to estimate a given number of sources. With two-way compression, the storage, handling, and transportation of the compactly designed UICSA is convenient, particularly for the AUVs with limited payload space. The deployment concept and process are discussed, as well as the various UICSA designs of different support structures are described. A comparison of the various mechanical designs is presented and a novel hybrid-based expansion prototype is documented in detail. Laboratory study results of the UICSA prototype are presented that include water-swollen material tests in a pressurized environment and water tank validation of the inflation process. The UICSA prototype also has been deployed in the Harbor Branch channel to validate the performance, the related field test details and source localization results.

**Keywords:** Underwater inflatable structure; Co-prime array; Structural design; Compressive sensing; Direction-of-arrival estimation; Field test.

---

### 1. Introduction

The state-of-the-art in recent underwater networking technology has been widely accepted and examined [1]. Underwater sensing networks (UWSN) are gaining traction as an effective means of measuring and monitoring ocean properties in situ. The UWSN employs sensor nodes and marine platforms, such as Remote Operated Vehicles (ROVs), unmanned surface vehicles (USVs), and Autonomous Underwater Vehicles (AUVs). Generally, a UWSN has three components: the master node, mobile nodes, and sensor nodes [2,3]. Node deployment consists of placing a certain number of sensor nodes in a designated area to collect data. Therefore, the systematic performances of the UWSN such as coverage, connectivity, and lifetime, will depend on this deployment. There are no general criteria when designing a sensor node deployment strategy. However, adjusting sensor detection range, communication radius, and other parameters in a suitable manner can yield a longer lifetime and greater network coverage. Master nodes are in charge of deploying the sensor nodes and controlling the network. The mobile nodes, mainly ROVs and AUVs, may carry sensor nodes and deploy or reconfigure them while simultaneously exploring and monitoring the environment. Once the nodes are implemented, the network topology is established and the routing policy and data transmission strategy of the network are set [4]. Sensor deployment is not only crucial to the functionality of the system, but it also represents one of the most significant cost inputs.

The other major cost is the price of the sensor nodes. Both are more expensive than those of terrestrial sensing networks [5]. Partan et al. predicted that UWSNs would mostly comprise high-cost nodes sparsely deployed over a large area [6].

With technological advances in underwater vehicles over the past decade, sensor deployment is now possible with ROVs or AUVs, leading to cost reductions. However, when using such vehicles for deployment, a sensor node must have a dimension that does not impose any physical restrictions on the vehicle itself and/or hinder its maneuverability [7]. As a result, developing compact deployable systems is crucial to conserving resources and ensuring the design simplicity of the deployment strategy. We recently proposed an Underwater Inflatable Co-prime Sonar Array (UICSA), with a novel Two-Way Compression (TWC) concept, as a deployable system carried by autonomous vehicles [8]. TWC involves dimensional compression and algorithmic compression. The dimensional compression employs an inflatable structure to reduce the initial physical volume as the array can be packed into low-volume containers carried by AUVs. The algorithmic compression is achieved through the use of a sparse array with hydrophone placement following the co-prime configuration and associated signal processing. Unlike the linear sonar array with uniform half-wavelength spacing, the co-prime array comprises two uniform linear subarrays having  $M$  and  $N$  hydrophones with specific inter-element spacings, with  $M$  and  $N$  being co-prime [9]. It offers  $O(MN)$  degrees-of-freedom for source direction-of-arrival (DOA) estimation.

The inflatable structure morphs into its final geometry after detaching from the carrier platform, such as an AUV. The morphing process is driven by a top buoy and weight/anchor at the bottom of the stowed package. The buoyancy and gravity straighten the entire array and maintain the desired hydrophone spacings. Different approaches can reinforce the stretched array and are presented in Section 2. The reinforced structure ensures the system rigidity and avoids being entangled, twisted, or bitten by marine life. The application of effective signal processing algorithms to the acquired datasets enables the localization of acoustic sources.

In this paper, we present the UICSA system concept in two narratives (mechanics and algorithm) in Section 2. The details of UICSA mechanical design are documented in Section 3. The UICSA prototype fabrication and laboratory validation experiments are outlined in Section 4. The initial field test of the UICSA conducted at the Harbor Branch Oceanographic Institute (HBOI) channel and performance evaluations of both narrowband and multi-frequency source estimation algorithms are presented in Section 5. Conclusions are drawn in Section 6.

## 2. UICSA system concept

A UICSA system is the integration of a co-prime array configuration with an underwater inflatable structure [8, 10]. Both components contribute to the initial compact system volume and low-cost construction.

### 2.1 Co-prime array and associated signal processing

A co-prime array configuration is obtained by interleaving two uniform linear arrays (ULAs), one with  $M$  hydrophones spaced  $Nd$  units apart and the other with  $N$  hydrophones having an inter-element spacing of  $Md$ .  $M$  and  $N$  are co-prime integers, and  $d$  is usually chosen to be one-half wavelength at the operating frequency [9]. The first hydrophone of the two ULAs coincide, resulting in a co-prime configuration with  $M + N - 1$  hydrophones. Under narrowband far-field operation, the co-prime array can be used for source DOA estimation. Multi-frequency operation, on the other hand, permits localization of near-field sources.

#### 2.1.1 Far-field narrowband DOA estimation

Let the positions of the hydrophones be denoted by  $x_i = n_i d, i = 1, 2, \dots, M + N - 1$ . Assume  $D$  narrowband sources are impinging on the co-prime array from directions  $\theta_1, \theta_2, \dots, \theta_D$ , with angles measured relative to the vertical axis. The received signal vector at snapshot  $t$  under far-field conditions can be expressed as

$$\mathbf{x}(t) = \mathbf{A}\mathbf{s}(t) + \mathbf{n}(t), \quad (1)$$

where  $\mathbf{A}$  is the  $(M + N - 1) \times D$  array manifold matrix whose  $(i, d)$ -th element is given by  $\exp(j\omega x_i \sin(\theta_d)/c)$ ,  $\omega$  is the frequency of operation,  $c$  is the sound speed in the water,  $\mathbf{s}(t)$  is the  $D \times 1$  source signal vector, and  $\mathbf{n}(t)$  is the  $(M + N - 1) \times 1$  noise vector. Assuming uncorrelated sources and spatially and temporally white noise, the  $(M + N - 1) \times (M + N - 1)$  covariance matrix of the received signal is given by

$$\mathbf{R}_{xx} = E[\mathbf{x}(t)\mathbf{x}^H(t)] \quad (2)$$

where  $E[\cdot]$  is the expectation operator and the superscript ‘ $H$ ’ denotes conjugate transpose. We note that, in practice, the sample covariance matrix is used in place of  $\mathbf{R}_{xx}$ . Vectorizing the covariance matrix  $\mathbf{R}_{xx}$ , we obtain the coarray observation vector

$$\mathbf{z} = \text{vec}(\mathbf{R}_{xx}), \quad (3)$$

which emulates a single snapshot received by a virtual array, known as the difference coarray [11, 12], whose element positions are the pairwise differences of the physical array hydrophone positions. Therefore, we can model the vector  $\mathbf{z}$  as [9]

$$\mathbf{z} = \tilde{\mathbf{A}} \mathbf{p} + \sigma_n^2 \tilde{\mathbf{I}} \quad (4)$$

where  $\tilde{\mathbf{A}} = \mathbf{A}^* \odot \mathbf{A}$ , with ‘ $\odot$ ’ denoting the Khatri–Rao product, is the coarray manifold matrix,  $\mathbf{p}$  is a vector containing the signal powers,  $\sigma_n^2$  is the noise variance, and  $\tilde{\mathbf{I}}$  is the vectorized version of an identity matrix. Using  $\mathbf{z}$ , sparse reconstruction methods [13, 14] or subspace techniques with interpolation [15, 16, 17] can be employed to fully exploit all degrees-of-freedom for source DOA estimation. We will use the former in this paper.

For sparse reconstruction, we first discretize the angular extent of interest into  $Q$  angles with  $Q \gg D$ . We construct a dictionary matrix  $\tilde{\mathbf{A}}$  to mimic the coarray manifold matrix corresponding to the  $Q$  discretized angles. We also define a  $D$ -sparse vector  $\mathbf{y}$  of length  $Q$ , whose  $q$ -th element indicates the presence or absence of a source in the direction  $\theta_q$ . Specifically, a zero-entry indicates the absence of the signal at angle  $\theta_q$ ; otherwise, the  $q$ -th element of  $\mathbf{y}$  is the source signal power from the corresponding direction. Then, the DOA estimation is accomplished by solving the optimization problem

$$\min_{\mathbf{y}} \|\mathbf{z} - \tilde{\mathbf{A}}\mathbf{y}\|_2^2 \quad \text{subject to} \quad \|\mathbf{y}\|_0 = D \quad (5)$$

where  $\|\mathbf{y}\|_0$  denotes the number of nonzero entries in  $\mathbf{y}$ . Since this optimization problem is NP-hard, we use orthogonal matching pursuit (OMP), which is a widely used algorithm that can approximately solve (5) [18].

### 2.1.2 Near-field multi-frequency source localization

For near-field processing, we present the signal model in the frequency domain. Considering  $D$  uncorrelated wideband sources located at  $\mathbf{x}_1, \dots, \mathbf{x}_D$  in the near-field of the array, the received signal vector corresponding to the  $q$ -th frequency can be expressed as

$$\mathbf{Y}(\omega_q) = \mathbf{A}(\omega_q)\mathbf{S}(\omega_q) + \mathbf{N}(\omega_q) \quad (6)$$

where the  $(i, d)$ -th element of  $\mathbf{A}(\omega_q)$  is  $e^{-j\omega_q \mathcal{D}_i(\mathbf{x}_d)/c}$ ,  $\mathcal{D}_i(\mathbf{x}_k)$  is the Euclidean distance between the  $d$ -th source and the  $i$ -th hydrophone,  $\mathbf{S}(\omega_q)$  is the source signal vector corresponding to the  $q$ -th frequency, and  $\mathbf{N}(\omega_q)$  is the white Gaussian noise vector at frequency  $\omega_q$ .

To coherently combine the received signals across different frequencies, we first pre-focus to some point  $\mathbf{x}$  in the near-field of the array by premultiplying with a matrix  $\mathbf{K}(\mathbf{x})$  [19, 20]

$$\mathbf{Y}(\omega_q, \mathbf{x}) = \mathbf{K}(\mathbf{x})\mathbf{Y}(\omega_q), \quad (7)$$

where  $\mathbf{K}(\mathbf{x}) = \text{diag}[K_1(\mathbf{x}), K_2(\mathbf{x}), \dots, K_{N+M-1}(\mathbf{x})]$  is the pre-focusing matrix with diagonal elements  $K_i(\mathbf{x}) = e^{j\omega_q \mathcal{D}_i(\mathbf{x})/c}$ . The covariance matrix of the pre-focused received signal is

$$\mathbf{R}(\omega_q, \mathbf{x}) = E\{\mathbf{Y}(\omega_q, \mathbf{x})\mathbf{Y}^H(\omega_q, \mathbf{x})\} \quad (8)$$

which is replaced by the sample covariance matrix in practice. The pre-focused covariance matrices are combined across different frequencies as

$$\mathbf{R}(\mathbf{x}) = Q^{-1} \sum_{q=1}^Q \mathbf{R}(\omega_q, \mathbf{x}). \quad (9)$$

If  $\mathbf{x} = \mathbf{x}_d$ , then the  $d$ -th column of  $\mathbf{K}(\mathbf{x})\mathbf{A}(\omega_q)$  equals  $\mathbf{1}_{N+M-1}$ , which is a vector of all ones and forms the steering vector of the pre-focused received signal [19]. Delay-and-sum beamforming at point  $\mathbf{x}$  with  $\mathbf{1}_{N+M-1}$ , therefore, yields a high response. Performing the pre-focusing procedure for all points of interest followed by near-field beamforming yields the output

$$P(\mathbf{x}) = \mathbf{1}_{N+M-1}^T \mathbf{R}(\mathbf{x}) \mathbf{1}_{N+M-1}, \quad (10)$$

with the superscript ‘ $T$ ’ denoting matrix transpose. The source locations are estimated by choosing the peaks of the beamformed output. High-resolution techniques can also be applied in lieu of beamforming for source localization [19, 21].

## 2.2 Vertical underwater inflatable structure

The underwater inflatable structure (UIS) is foldable and can morph into a large span, also referred to as underwater deployable structure or ocean morphing structure [8,10,22,23]. The UIS contributes to the dimensional compression of UICSA with the initial folded structure. This folded structure can be packed into a low-volume container for storage and transportation, ideal for AUVs with the limited payload space. After detaching from the carrier platform, the container packed with UICSA needs to release the entire system to guide the morphing process of the UIS. The feasibility of a horizontally-oriented UIS has been discussed in [8], where the self-contact forces drive the morphing process during UIS expansion.

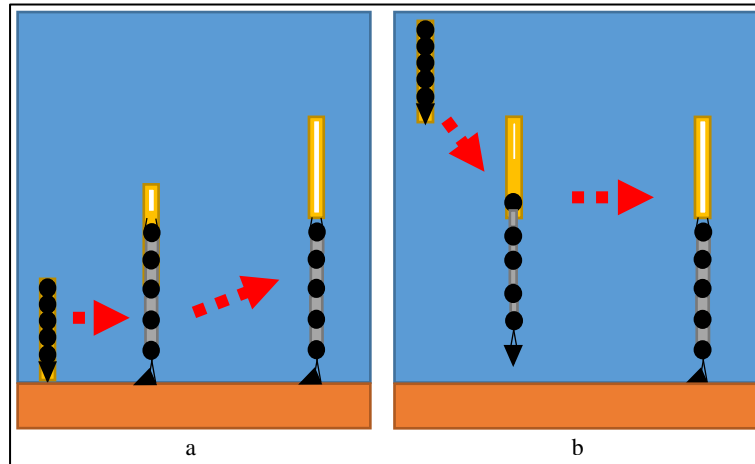


**Figure 1.** Vertical UIS release methods during morphing: (a) Lift method; (b) Drag method.

In this paper, we focus on the vertically-oriented tubular UIS, with the morphing process driven by buoyance at the top and gravity at the bottom. The packed UICSA container remains negatively buoyant and keeps sinking towards the seafloor. Figure 1 demonstrates two practical methods to release the UIS from a container, namely, the lift method and the drag method. In the first design, the top buoy lifts the UIS from the container after the system anchors on the seafloor. In the second design, the weight/anchor drags the UIS out of the container during the sinking process. The lift method requires the package settlement first and then releases the buoy for morphing, which may lead to a longer morphing process. On the other hand, the drag method can complete the morphing and even can start inflation during the sinking process. However, the morphed structure is susceptible to the currents during the sinking process and can drift from the desired destination. Therefore, the lift method can cope better with strong currents, whereas the drag method is better suited for expeditious deployment in calm waters. The primary focus of this paper is the UIS system design suitable for calm shallow coastal water (around 100 to 150 m depths). The UICSA design for more challenging conditions (i.e., deep water and under strong current) will be reported in future work.

After the morphing process, UIS requires reinforcement to strengthen the array and keep the embedded hydrophones at the correct spacing under the influence of ocean currents and marine life. The reinforcement process involves swelling actions within the UIS. The UIS infill expansion provides the tension of tubular structures, secures hydrophone positions, and also ensures system resilience. The expansion process can be achieved by various approaches involving different structural designs and materials, as discussed in Section 3.

## 2.3 Underwater Deployable Sensing Network (UDSN)

One of the overarching goals of the UICSA project is to develop the concept of an underwater deployable sensing network (UDSN). A UDSN will consist of multiple UICSA nodes to detect and track the target within the water volume under surveillance. Figure 2 demonstrates the UDSN concept where the UICSA nodes are deployed from a USV, an AUV, and a helicopter. Each UICSA, as a node of the UDSN, records acoustic emissions from sources in the covered volume and relays them to the surface asset via acoustic links. The on-board processing of the surface vehicle can apply associated algorithms to the acquired signals and send the resulting source estimates to the satellite, helicopter, and/or command center. In this way, the UDSN can collect a set of high-quality transient acoustic data over a span of locations as a sufficiently transformative UWSN.

One novelty of the UICSA design is that it realizes the TWC concept by combining the aforementioned compression methods. The sparse array requires fewer hydrophones than a linear array to provide the same resolution, which reduces the fabrication cost and initial volume. The UIS design provides the required rigidity regardless of the tension provided by the buoy and weight/anchor. By utilizing TWC, the UICSA in its deflated form can be folded and packed into reduced forms for handling, storage, and conveyance. The compact UICSA package can not only fit the limited payload capacity of AUV/USV but is also adaptable to existing watercraft as well as packed into a sonobuoy and released from airborne platforms, such as helicopters. The UICSA has advantages over towed sonar array in terms of vessel capability, and Size, Weight, Power, and Cost (SWaP-C) constraints. After the UICSA completes the morphing and reinforcing processes at the deployed location, it can start data collection as a node of the UDSN. The acquired data can be relayed to the ship-borne or onshore processing center via a hybrid of underwater acoustic links and radio links above water. Moreover, it is practical and almost effortless to increase the UDSN resolution with more UICSA-based nodes deployed from AUVs.

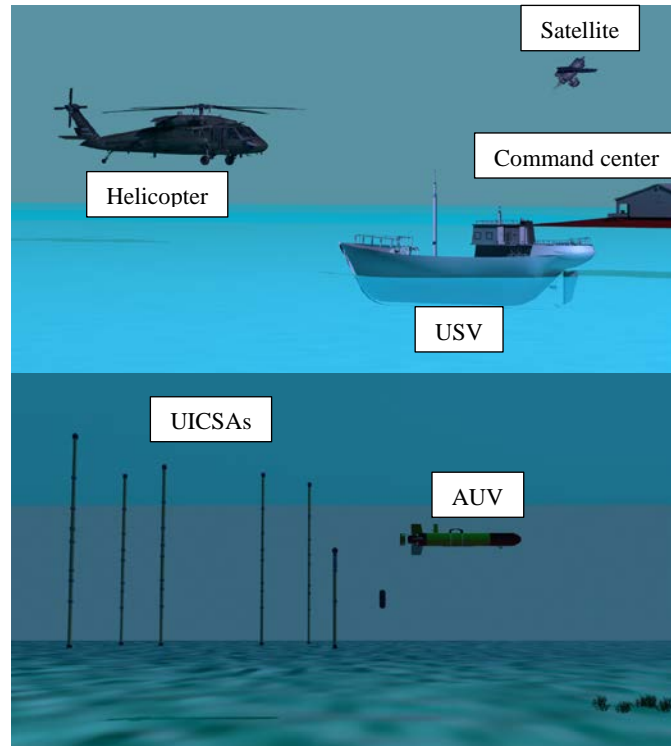


**Figure 2.** Underwater Deployable Sensing Network (UDSN).

### 3. System design and prototyping

The UICSA needs to satisfy the initial compact volume constraint to accommodate the limited payload space of AUVs. After detachment from AUVs, the deployed UICSA needs to complete the morphing process smoothly and achieve the final stage, in a short time, to start data collection.

The fully implemented UICSA is also required to minimize the effects of structural deflections, vibrations, and entanglements due to ocean currents and marine animal activities. In this section, we present the vertical UICSA prototype design, detailing the dimensions and applied materials.

#### 3.1 Dimensions of the UICSA prototypes

The UICSA length is determined by the operating acoustic signal frequency and the desired upper limit on the number of resolvable sources. The signal frequency defines the unit length,  $d$ , whose maximum value equals half-wavelength at the operating frequency. The overall structure length is determined by the specific choice of  $M$  and  $N$  values to meet the source number constraint, together with the chosen unit length. In this study, we select 2.5 kHz as the operating frequency in the prototyping effort, which corresponds to a wavelength of  $\lambda = 0.6$  m for 1500 m/s sound speed in the water. We consider two different UICSAs, namely, a 4-element ( $M = 2, N = 3$ ) array with  $d = 0.5\lambda$  and a 7-element ( $M = 3, N = 5$ ) array with  $d = 0.2667\lambda$ , as shown in Figure 3. The 4-element array can resolve up to 6 acoustic sources, while the maximum number of estimated sources increases to 15 for

the 7-element array. In contrast, a ULA would require 7 and 16 sensors, respectively, to resolve the same number of sources as the corresponding co-prime arrays.

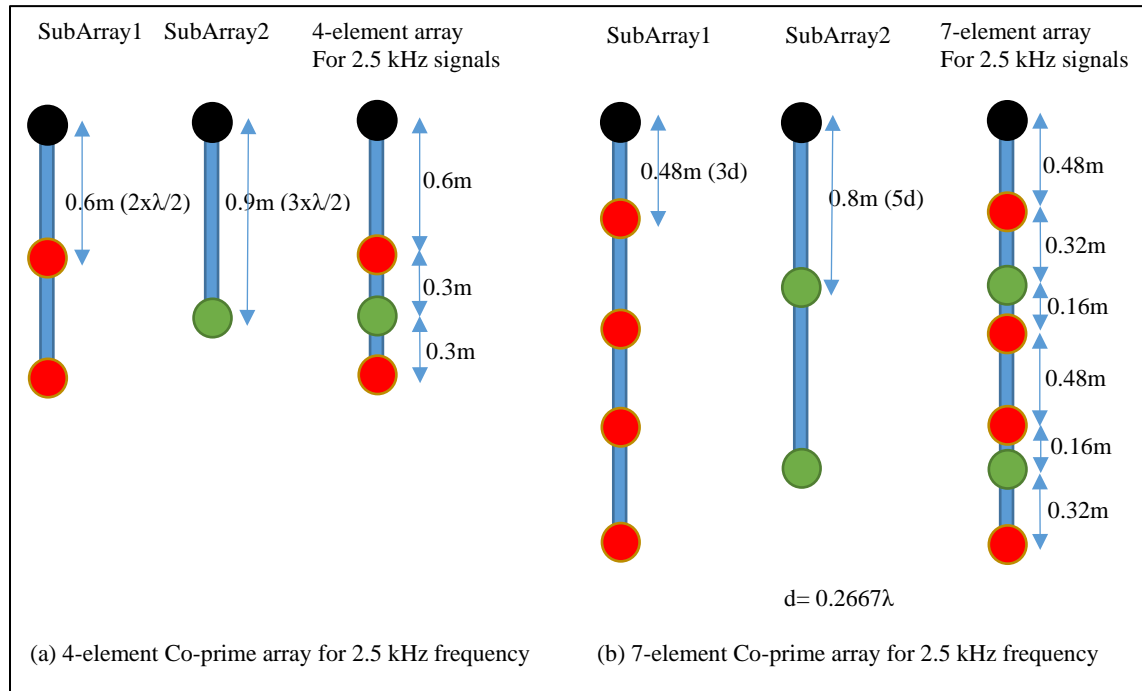


**Figure 3.** (a) 4-element and (b) 7-element UICSA prototypes, operating at 2.5 kHz.

### 3.2 Energy-efficient UIS techniques for UICSA

The vertical UICSA is designed to be fully stretched by weight tethered to the tail and a float attached to the top. After completion of the morphing process, UICSA requires reinforcement to maintain the structural rigidity through the expansion within the array structures themselves.

#### 3.2.1 Mechanical-based Expansion (MBE) approach

The MBE approach was initially evaluated in the UICSA design [10]. It employs the hydraulic inflation method to complete the swelling process. The MBE design requires a watertight tubular structure and water injection into the UIS by an underwater pump. The hydraulic pump can inflate the fabric in a matter of minutes and keep the UIS at appropriate stiffness to mitigate deflection under ocean currents. In the MBE design, the injection point is usually at the bottom of the UIS with a vent orifice on the top. The proposed mechanism stabilizes the UIS during the morphing and expansion processes, as the pump provides the force to keep UIS rooted on the seafloor, and the vent permits restrained air to move along the structure during the injection process.

For the tubular UIS design, we divide the structure into sections of lengths equal to hydrophone spacings to ensure the feasibility of the prototype. The waterproof ploy film (0.15 mm thickness) is selected to fabricate the UIS. The impulse heat sealer (Metronic 400 mm manual sealer) is applied to seal the closure along the UIS axial direction. The ends are sealed by tube fittings and holding rings with NPT female threads. The top-end connects with the pressure relief valve for ventilation, while the bottom end is fitted with a barbed tube fitting for water injection. The tubular sections and connectors are cemented together using epoxy. The components applied in the prototype are built for tank test and concept verification. For deep-water deployment, the MBE UICSA requires an applicable deep-water pump and certified components.

However, the MBE design has some shortcomings. The pump needs to run continuously during expansion and then periodically to maintain the UIS stiffness. The energy consumption required to support the pump operation may be especially problematic for any long-endurance monitoring missions. The pump also requires a substantial battery pack, which increases the size and mass of the UICSA system. In addition, the pump operation generates vibrations and noise, which serve as sources of interference during data collection. For this reason, we investigated other more energy-efficient UIS approaches.

#### 3.2.2 Chemical-based Expansion (CBE) approach

The CBE UICSA design employs a watertight tubular structure and expandable chemical resins as infilling to swell and strengthen the UIS. As the UIS stiffness is achieved by chemical reactions between the mixture synthetic

resins, it only requires a smaller battery pack to power the mixing process and the expansion within a relatively shorter period. The CBE design eliminates the bulky battery required for the MBE design. One type of material that has been evaluated for CBE design is HMI HF402 HydroFOAM [25]. The HF402 HydroFOAM is hydro-insensitive polyurethane foam, which can form high-quality foam even when submerged in water. HF402 begins with two-part pair resin and can be mixed to trigger the reaction. During a small-scale laboratory test with a  $100 \times 25$  mm flat tube, the hydrofoam sustained the injection, reaction, and curing phases. The underwater expansion process took 45s and swelled seven-times compared to the initial volume. The foam can completely cure within 5 minutes in an environment at 21 to 28 °C. Since the cured hard solid tube has uniform infill and maintains its volume, there is no need for additional action once the expansion of the UIS is complete, which is an advantage over the MBE design. While the CBE bead structure can be recovered after the mission is over, the sensors and other components will need to be removed from the expanded and solidified foam and repackaged for redeployment. In this regard, the CBE design is more suitable for disposable, single-mission deployment using low-cost hydrophones and electronics. For applications requiring re-deployable UICSA, two other designs, namely, physical-based expansion (PBE) and hybrid-based expansion (HBE), are applicable, which are discussed below.

### 3.2.3 The PBE approach

The PBE design utilizes water swelling material (WSM) as infilling to achieve expansion after morphing. The WSM absorbs water molecules with volume expansion. One typical WSM is a hygroscopic gel (hydrogel), which can grow to over 250 times its initial volume [23]. Hydrogel, a superabsorbent polymer (polyacrylamide and polyacrylate), can shrink back to its initial volume through dehydration, which leads to a recoverable array design. With the presence of the hydrogel, the PBE design can accomplish the expansion process independently without any energy cost or additional actions after the UIS is pulled out of the packaging container.

Unlike the MBE and CBE, the current PBE design employs a permeable tube for the UIS to allow WSM contact with the surrounding water. Hydrogel beads are utilized as infilling of the nylon sleeve forming the UIS. The hydrogel beads are made of condensed superabsorbent polymer and the swelling speed is relatively slow which takes several hours to finish the expansion process. In contrast, both the MBE and CBE designs are capable of full expansion within several minutes. In general, the PBE design is practical for small diameter nylon sleeves where reasonable stiffness can be achieved within one hour. However, the rigidity of small cross-section nylon sleeves was found to be lacking for larger-span structures. To resolve these issues a hollow pipe-shaped design is employed. In this design, a set of small diameter nylon sleeves is combined to form a panel. The panel can then be rolled to form a large diameter pipe, as shown in Figure 4. Such PBE design permits more surface area to have contact with water and expands quicker than the one made of a large diameter sleeve.

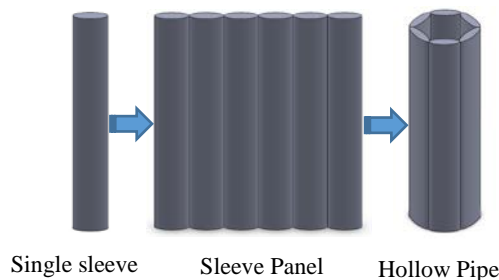


**Figure 4.** Nylon sleeve hollow pipe design.

Both the single tube and hollow pipe-shaped PBE based UIS requires longitudinal uniform infilling. If the beads are placed unconstrained inside a vertical UIS, it will have a solid lower section but insufficient rigidity in the upper section. Based on this finding, a narrow column made of water-soluble paper is introduced to store the dry beads and ensure an even distribution along the length of the structure. After the structure comes into contact with water, the restriction is lifted, permitting the beads to grow while staying at a pre-set stacking location along the array length.

### 3.2.4 The HBE approach

We summarize the advantages and limitations of MBE, CBE, and PBE designs in Table 1, where the red blocks represent restrictions, the acceptable conditions are marked in yellow, and the advantages are shown in green. We note that all three designs have limitations to create a compact, rapidly deployable, and recoverable UICSA. In particular, the PBE design may take an hour or longer to complete the expansion, and is prone to entanglements and twisting due to ocean currents and marine life. These issues motivated us to investigate an HBE design.

Specifically, we integrate MBE and PBE concepts to build an HBE UIS, which can complete the initial expansion in a short time and reduce energy consumption to maintain structural stiffness.

The proposed HBE design is a hybrid of external MBE and internal PBE configuration. The outer and inner layers are attached at both ends to ensure morphing synchronization. The PBE based UIS can achieve rigidity rapidly with water injection after fully morphed, and it maintains rigidity through the built-in expanding PBE structure.

**Table 1.** UIS design benefits and detriments

UIS Designs	MBE	CBE	PBE
Initial volume	Large	Small	Small
Initial weight	Heavy	Light	Light
Initial Expansion speed	Quick (< 10minutes)	Quick (< 10 minutes)	Slow (> 1 hour)
Power consumption	Bulky battery	Not required	Not required
Maintenance After Expansion	Period inflation required	No	No
Generated Noise	Pump inflation	No	No
Expanded structure	Thin-film tube	Rigid beam	Semi-rigid beam
Recoverability	Yes	No	Yes



**Figure 5.** HBE design expansion process

Figure 5 describes the expansion process of HBE based UIS. The HBE UIS requires materials including watertight films as an external layer, permeable fabrics as an internal layer, and WSM as infill for expansion. The outer layer ensures water retention after the initial expansion through water injection. After the initial pump injection, the flat structure turns into a thin-wall tube containing internal pressurized water. It maintains certain stiffness against external forces. In the meantime, the inner layer is permeable to allow water contact with contained WSM and starts the moderate expansion. The internal PBE layer eventually turns into a solid beam after full expansion and reinforces the rigidity during data collection.

The HBE design employs a hydraulic approach to accomplish initial expansion, similar to the MBE approach. However, it eliminates the periodical inflation required in the original MBE design after the initial expansion as the internal PBE layer starts to swell. Theoretically, the WSM can absorb water within the watertight external layer and continue the absorption with given access to the surrounding water. Since the pump is only required for initial injection, a smaller battery pack may be employed to support the initial pump operation and hydrophone data acquisitions. Therefore, the initial package volume, mass, overall energy consumption, and cost can be significantly reduced compared to the original MBE design.

In addition to the reduced energy consumption, the HBE design is more robust than MBE against punched holes or leakage in the sealed layer. As the HBE’s eventual rigidity is determined by the internal layer, the leaked external layer only affects expansion speed and the HBE based UIS can subsequently reach the predetermined rigidity with full expansion. The applicable depth for the HBE design depends on the applied components of the MBE design for initial expansion and the infilled WSM of the PBE design for maintaining the final geometry.

#### 4. System prototyping and validation tests in laboratory

In this section, we report on the HBE based UICSA material evaluation, prototype fabrication details, and deployment in laboratory tanks.

##### 4.1 Pressure test of materials

To minimize the initial volume of the HBE based UICSA, we select hydrogel beads as the WSM infillings. The hydrogel beads are made of condensed superabsorbent polymer, so the swelling speed is relatively slow compared

to the powder. In preliminary tests, it took several hours for the UIS to expand and achieve a reasonable stiffness after deployment [23].

Since the UICSA is designed for deployment in shallow coastal water at around 100 to 150 m depth, we evaluated the hydrogel beads performance in a similar ambient environment with a water pressure chamber which is shown in Figure 6(a). During the test, we placed hydrogel beads of different colors in the sealed chamber as illustrated in Figure 6(b), then pressurized the chamber to reach 1241 kPa (equivalent to 125 m depth) with the help of a dial indicator, as shown in Figure 6(c). We maintained the pressure level for six hours to observe the performance of the beads through the viewport. We also placed one set of beads in a water cup under normal pressure as a controlled trial; the beads took eight hours to fully expand, as shown in Figure 6(d). Interestingly, we noticed that the beads in the pressurized tank fully expanded in about one hour, as seen in Figure 6(e). Compared to the eight hours for the submerged beads to achieve full expansion under normal pressure, an increase in the ambient pressure accelerates the swelling process. The diameters of the swollen beads were roughly 15.8 mm, as presented in Figure 6(f). We also opened and retrieved the swollen beads after six hours and compared their measurement with the dry beads as shown in Figure 6(g). The diameters of the dry beads are approximately 3.2 mm and those of the swollen beads are 14 mm roughly. Therefore, the diameters of the fully swollen beads were at the same level regardless of the applied pressure. The results demonstrate that the hydrogel beads can swell in a shorter time under pressure, maintain integrity for a long time, and provide about 80 times volume expansion.

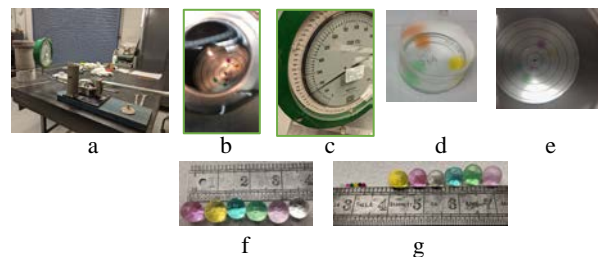


Figure 6. Hydrogel beads pressure chamber test

#### 4.2 UICSA prototype design

We fabricated the UICSA prototypes in compliance with the designs elaborated above. Specifically, four different prototypes were developed: a 7-element MBE-based UICSA, 4-element and 7-element PBE based UICSAs, and a 7-element HBE based UICSA [10, 24]. Most components applied in the UICSA prototyping process were built through fused deposition modeling (FDM). The parts required to be watertight were coated with epoxy. In the interest of brevity, we only present the details of the 4-element HBE based UICSA prototype; the details of other prototypes are documented in [10, 24].

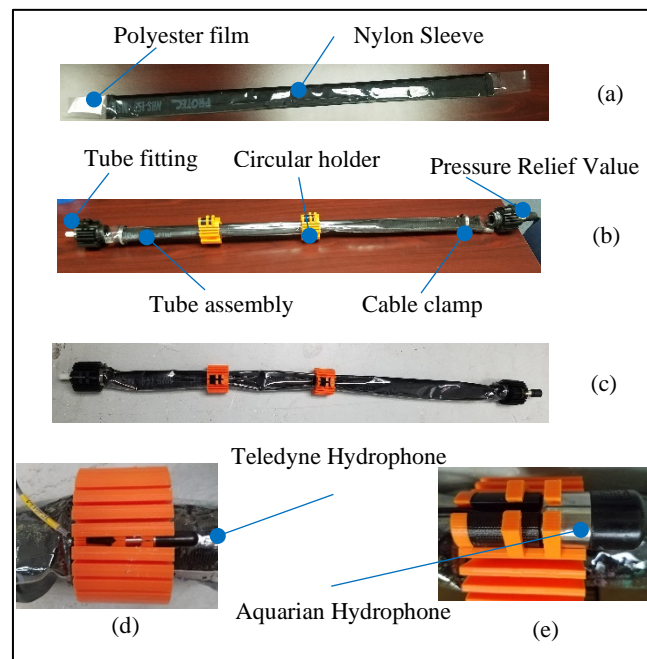
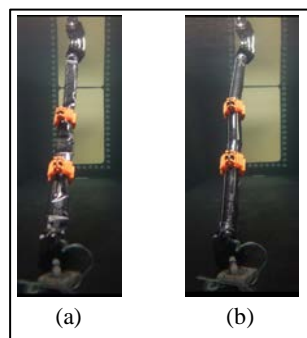


Figure 7. 4-element HBE based UICSA structural details

The tubular structure assembly of the 4-element HBE based UICSA comprised two tubes: the external tube made of watertight Polyester film, and the internal tube made of Nylon sleeve filled with WSM- dry hydrogel beads, depicted in Figure 7(a). The outer tube was attached to the inner tube at both ends using glue. The internal tube contained dry hydrogel beads stored in a string of soluble paper bags. The HBE based UICSA consisted of circular holders, tubular structure assembly, cable clamps, barbed tube fitting, and pressure relief valve, as shown in Figure 7(b). The external tube is sealed at both ends, leaving one end connected with barbed tube-fitting for water inflation and the other with a pressure relief valve for trapped gas ventilation. Figure 7(c) depicts HBE based UICSA with both ends sealed and tightened by cable clamps, while the remaining holders are glued to the external tube. The applied circular holder is designed to carry two types of hydrophones (Teledyne RESON TC 4013 [26] and Aquarian H2a [27]). Figures 7(d) and 7(e) show the circular holder carrying Teledyne and Aquarian hydrophones, respectively.

### 4.3 Validation of prototype expansion after deployment

Having validated the UICSA morphing process with the MBE-based UICSA and the expansion performance after being entirely morphed for the PBE based prototypes, as reported in [10] and [24], we conducted the feasibility test of the 4-element HBE based UICSA.



**Figure 8.** 4-element HBE based UICSA expansion process

Figure 8 presents the expansion process of the 4-element HBE based UICSA. The prototype required an underwater pump at the bottom end for water injection, while the top end needed to be connected with an opened pressure relief valve to allow the flow from bottom to top and to ensure that the internal nylon sleeve is submerged. The bottom end was also tethered with weight and the top-end secured with a crossbar over the water tank to keep the array stretched. Because the water tank was not deep enough, we had to tilt the UICSA to ensure that the structure remained below the surface. Figure 8(a) reveals the initial state of the structure, which is flat and slack. Once the pump started to inject water into the array, the UICSA became stiffer due to the pressure difference. Then, the hydrogel beads grew to a large volume and reinforced the structure stiffness, as seen in Figure 8(b). After complete expansion UICSA can operate as a sensing node.

After the validation of the prototype expansion process, we also conducted a numerical study to understand the performance of the fully expanded UICSA structure under external forces, such as ocean currents. Because the HBE based UICSA stiffness is contributed by the MBE-based structure at the beginning and later by the PBE based structure, we deduce that a fully expanded HBE based structure demonstrates the same structure response as the PBE base UICSA with the same dimensions. As such, we only created numerical models of MBE, CBE, and PBE based UICSA's tethered with a buoy on the top and moored on the seafloor. Based on the simulation results in OrcaFlex [28], although all of the considered UICSA's drift along the direction of the ocean current with a slight curvature along the array length, they all maintain the hydrophones at the correct relative locations under the small current conditions. This implies that the UICSA should work properly as a sonar array for source estimation [29]. To assess the design and validate the simulation results under realistic conditions, we conducted a field deployment in the presence of underwater flow and marine animals, as described in the following section.

## 5. The initial field validation experiment

### 5.1 Prototype field deployment in HBOI Channel

In this initial field experiment, we deployed a fully expanded 7-element PBE based UICSA, because the fully expanded HBE UICSA has the same structural stiffness as the PBE design. We previously employed the same PBE based UICSA prototype in an acoustic test tank for data collections [24]. After the acoustic test tank experiment, the prototype was retrieved from the acoustic test tank and left in a dry environment for dehydration. Once the infilling shrank back to its initial volume, the UICSA was packed and stored in a container. Using the

same prototype in the field experiment, thus, also provides an opportunity to test the reusability of the UICSA after dehydration of the hydrogel beads.

The total spacing from the first hydrophone to the last hydrophone is 1.92 m for the 7-element UICSA. However, the actual structure length is fabricated to be 2 m, leaving space on both ends for lift and weight installation. We selected the HBOI channel as the initial field test site instead of fully open water, such as the Indian River Lagoon or Atlantic coastal area. The primary consideration for this choice was to reduce the complexity of the field test. The Harbor Branch channel outlet connects to the Indian River Lagoon, as shown in Figure 9(a), and introduces the currents from the East to the West. To avoid multipath arising from the floor/walls, the deployment site depth needs to be over 4.5 m. The majority of the channel depth is about 4 m, which only leaves three possible locations for deployment in front of the dock area, marked as Sites A, B, and C in the hydrographic map of Figure 9(b), where the depth is marked in feet. The boat employed for array deployment could drift under the waves, currents, and wind during the field test. To mitigate such effects, the boat needed to be tied to the seawall post. As such, Site C turned out to be the best option because of its close proximity to the seawall at 8 m away, thereby permitting the HBOI research vessel (Harbor Branch Pontoon #2) of 7.5 m length to reach this site while tied to the seawall post. The purple pentagon marked in Figure 9(b) represents the Pontoon #2 parked perpendicular to the seawall with the bow reaching Site C.

The channel also serves as a habitat for marine animals, such as dolphins, groupers, and manatees. As the UICSA is a passive array, it is necessary to deploy an active sound source during the field test operating at a center frequency of 2.5 kHz. This frequency is within the hearing spectrum of dolphins and manatees. To avoid causing any harm to marine mammals, the power of the sound source is required to be below 60 dB. As the embedded Aquarian H2a hydrophone can distinguish the sound over ambient noise within 15 m range, the speaker has to be deployed from the boat instead of a far-field location.

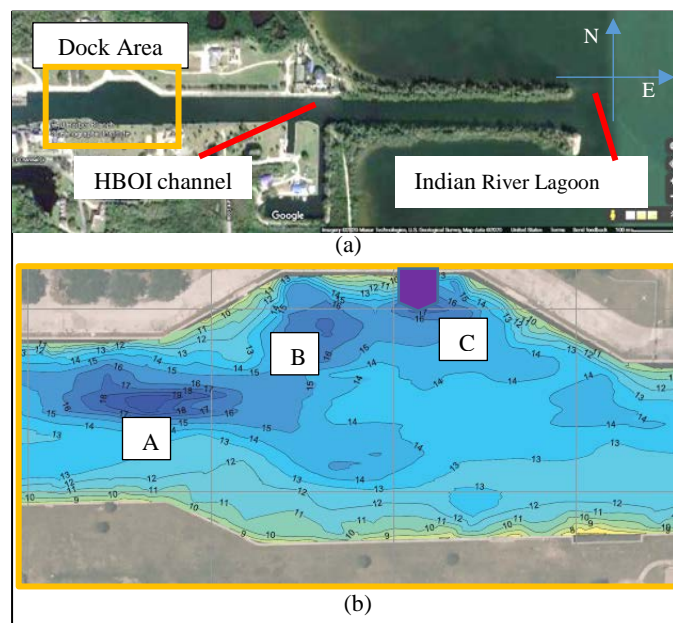


**Figure 9.** HBOI Channel and site selection.

We also had a time constraint since the test was to be completed in the channel within a four-hour window. Therefore, it was impractical to deploy the flat 7-element PBE based UICSA, which requires hours to reach the desired stiffness. Consequently, we pre-expanded the prototype in the Systems and Imaging Lab (SAIL) indoor tank overnight and examined it to ensure that the desired stiffness was achieved before the field test.

We loaded the re-expanded array on Pontoon #2, shown in Figure 10 (a). During the test, the boat was anchored using a three-point mooring to mitigate drifting. Two fluke anchors tethered to the bow of the boat were deployed in the channel. The stern was tied to the post next to the seawall. Figure 10 (b) shows Pontoon #2 traveling across the channel to deploy the anchors. After the front two anchors were deployed, Pontoon #2 was moved backward to reach the seawall post to fasten the stern perpendicular to the seawall. After the boat was anchored, the bow reached Site C with the 5.18 m depth. Using a marked rope, the array was deployed with the first hydrophone at 1 m depth below the surface. Figure 10(c) shows the UICSA deployed from the Pontoon #2. After the array was secured at the desired depth, an INSMY IPX7 waterproof speaker [30] was deployed from predetermined locations around the boat at a 0.5 m depth, pointing towards the array. The experimental layout for the acoustic tests is shown in Figure 10 (d). The red dots denote the speaker's locations, and the yellow dot indicates the array position.

At each location, we collected two sets of measurements; a monochromatic measurement where the speaker played a looped 2.5 kHz single tone, and a multi-frequency measurement with the speaker emitting a chirp signal of bandwidth 300 Hz centered at 2.5 kHz. The data were recorded by the deployed array using two Zoom H6 data loggers [31] with a sampling frequency of 96 kHz. The current data loggers are not submersible and require manual operation for data acquisition. For comparison, we also deployed a 7-element co-prime array on a rigid structure and repeated the same experiments as that for the UICSA prototype. During the field deployment, we observed that in chirp measurements with the rigid array, the hydrophone marked in black in Figure 3(b) malfunctioned.

**5.2 Acoustic performance using the field experimental data**

To validate the acoustic performance of the UICSA, we processed both the single tone and the chirp measurements from the field test. The signal model detailed in Section 2.1.1 deals with far-field measurement conditions. Due to the constraints imposed by the channel dimensions, the speaker positions 1, 2, and 5 in Figure 10 (d) are closer to the array and, thus, exhibit a much higher deviation from the far-field source approximation compared to positions 3 and 4. Therefore, these were excluded from performance evaluation for the case of 2.5 kHz single tone data. On the other hand, for near-field source localization with the chirp signals using the method discussed in Section 2.1.2, we considered speaker positions 1 and 2 only.

Table 2 shows the nominal DOA for speaker positions 3 and 4 based on the ground truth, with  $\theta_t$  and  $\theta_b$  denoting the respective directions of the speaker relative to the top and bottom hydrophones of the co-prime array and  $\bar{\theta}$  being the average DOA. Ideally, the angular spread across the array should be zero under far-field conditions. Although the considered speaker positions do not satisfy the exact condition for the far-field source, nonetheless, we expect reasonable estimation accuracy with far-field processing. Since only a single acoustic source was present per experiment, we employed OMP with a sparsity level set to 1 for DOA estimation. For both the UICSA and the rigid array, we used measurements from speaker position 3 for calibration and retained the same calibration for processing data from position 4. The last two columns of Table 2 provide the resulting DOA estimates for the UICSA and the rigid array, respectively, while the corresponding normalized OMP spectra are depicted in Figure 11. We observe that, for each speaker position, the estimated DOA using both arrays falls within the corresponding nominal angular spread and is close to the corresponding average DOA. These results corroborate that the UICSA provides similar performance to that of a rigid co-prime array.

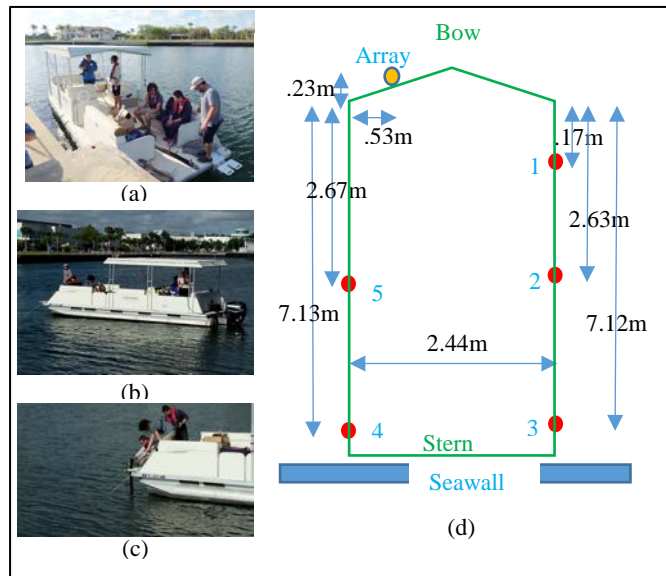


**Figure10.** Field test setup.

**Table 2.** Nominal and Estimated Source DOAs.

Speaker	Nominal DOA (deg)			DOA Estimate (deg)	
	$\theta_t$	$\theta_b$	$\bar{\theta}$	UICSA	Rigid
Position 3	3.77	17.68	10.72	10.54	10.72
Position 4	3.88	18.16	11.02	12.88	9.64

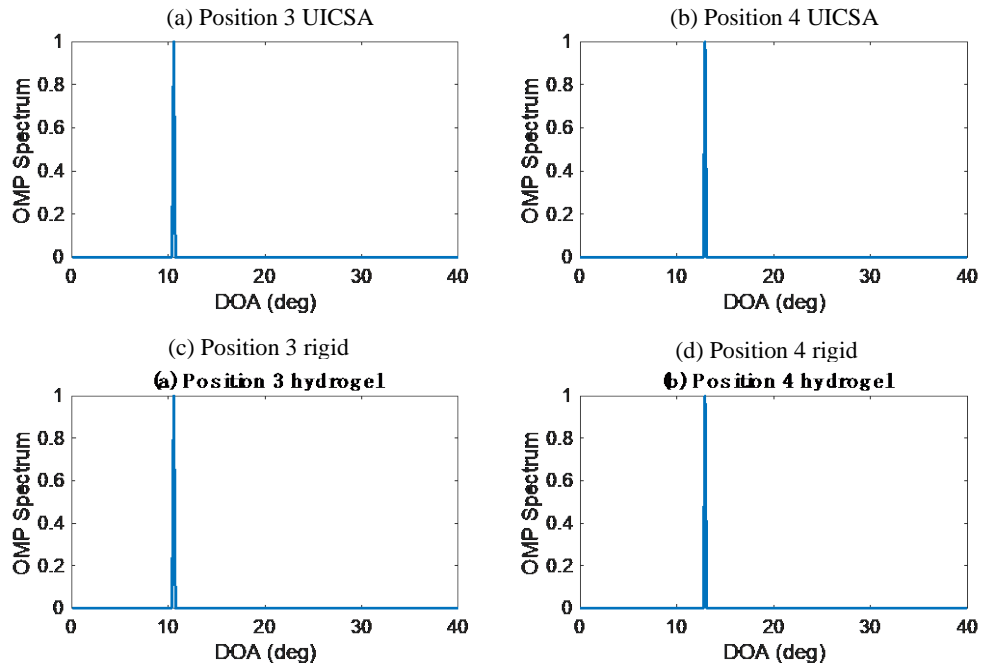


Figure 11. Normalized OMP spectra.

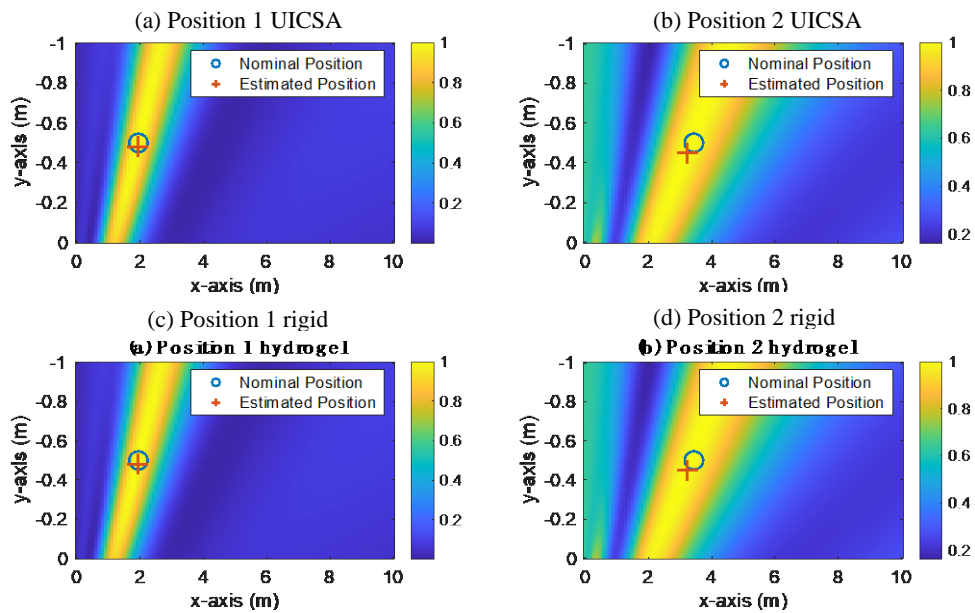


Figure 12. Normalized near-field beamforming spectra.

For near-field processing with both UICSA and the rigid array, the data from position 1 is used for calibration, and the same calibration is retained for processing the data from position 2. The normalized near-field beamforming spectra are depicted in Figure 12 where the true source positions are marked with “o”. The array is aligned along the positive y-axis. At a propagation speed of 1500 m/s for sound in water, the range resolution is 5 m for the 300 Hz bandwidth, causing the main lobe to be extended in range. However, the peak intensity value, which is the source location estimate and marked as “+” in Figure 12, is very close to the ground truth for the UICSA. For the rigid array, only position 1, which is self-calibrated, is accurately estimated. For position 2, although the direction of the source is resolved, the location estimate exhibits a large bias. This is caused by the malfunctioning of the first hydrophone. The specific hydrophone is said to be essential for reliable processing since the deletion of this hydrophone results in a reduction of the degrees of freedom offered by the co-prime array [32]. As such, its loss due to malfunctioning leads to erroneous estimate by the rigid array.

## 6. Discussions and conclusion

In this paper, we investigated various aspects of UICSA, including concept validation, design, prototyping, laboratory validation tests, and field performance tests. The UICSA deployment strategy was documented and validated with tests. The UIS design concept with four different approaches, namely, MBE, CBE, PBE, and HBE, was detailed. The HBE based UICSA prototype was fabricated and deployed in SAIL tank, which validated the HBE prototype's performance as proposed. Besides, we also validated the HBE UICSA related infilling WSM's performance, which can swell and maintain its integrity at 125m depth in the pressure chamber test. Using measurements with a PBE design in field tests, we demonstrated that a UICSA could accurately estimate sources.

The current prototype was developed to validate the proposed concept. As such, some components will need further development to be ready for field tests in deeper water. For example, the data acquisition device cannot operate underwater and the 3D-printed holders are not suitable for deep water. The next-generation prototype needs to be fully submersible and configured to acquire data automatically. Further development is required in terms of the design of a new control device together with the hydrophones fully embedded within the HBE UIS to reduce the initial volume, along with other required components including battery and pump, to fit the compact deployable container. We also envision further improvements in the structural designs, enhanced processing methods to address sound speed ambiguities and hydrophone positioning errors under large current conditions, and performance validations using field tests under more challenging environments. Moreover, we plan to extend the proposed UICSA designs to two-dimensional sonar array configurations. We also aim to expand the UIS concept to other ocean engineering applications, like marine animal detection and surveillance task.

## 7. Acknowledgements

This work was supported in part by the Office of Naval Research grants N00014-18-1-2460 and N00014-18-1-2469, National Science Foundation REU programs 1659484 and 1659468, HBOI Foundation summer internship program, and HBOI Foundation Research Excellence fund. The authors appreciate Dr. Michael Traweek for his suggestions on the initial HBE concept, Mike Young, Nathan Newell, Jimmy Nelson, and Matt Roy for operating the HBOI research vessel during the field test. The authors would also like to extend our thanks to Mike Young, Guifang Tang, Casey De Ouden, and Dr. Georgios Sklivanitis for the assistance during the lab tests, and OrcaFlex for offering the simulation software resources.

## 8. References

- [1] Chitre M, Shahabudeen S, Stojanovic M. Underwater Acoustic Communications and Networking: Recent Advances and future challenges. *Marine Technology Society Journal*. 2008;42(1):103–116.
- [2] Sheikh AA, Felemban E, Felemban M, Qaisar SB. Challenges and opportunities for underwater sensor networks. 2016 12th International Conference on Innovations in Information Technology (IIT). 2016.
- [3] Heidemann J, Ye W, Wills J, Syed A, Li Y. Research challenges and applications for underwater sensor networking. *IEEE Wireless Communications and Networking Conference, 2006 WCNC*. 2006.
- [4] Wei Z, Song M, Yin G, Wang H, Ma X, Song H. Cross deployment networking and systematic performance analysis of Underwater Wireless Sensor Networks. *Sensors*. 2017;17(7):1619.
- [5] Tuna G, Gungor VC. A survey on deployment techniques, localization algorithms, and research challenges for Underwater Acoustic Sensor Networks. *International Journal of Communication Systems*. 2017;30(17).
- [6] Partan J, Kurose J, Levine BN. A survey of practical issues in underwater networks. *ACM SIGMOBILE Mobile Computing and Communications Review*. 2007;11(4):23–33.
- [7] Vasilescu I, Kotay K, Rus D, Dunbabin M, Corke P. Data collection, storage, and retrieval with an underwater sensor network. *Proceedings of the 3rd international conference on Embedded networked sensor systems - SenSys '05*. 2005.
- [8] Ouyang B, Li Y, Zhou T, Su T-C, Dalglish F, Dalglish A, et al. Compressing two ways: The initial study of an underwater inflatable co-prime sonar array (UICSA). *Compressive Sensing VII: From Diverse Modalities to Big Data Analytics*. 2018.
- [9] Vaidyanathan PP, Pal P. Sparse sensing with co-prime samplers and arrays. *IEEE Transactions on Signal Processing*. 2011;59(2):573–586.
- [10] Li Y, Ouyang B, Dalglish F, Dalglish A, Su T-C, Baver S, et al. Mechanical design consideration of an underwater inflatable co-prime sonar array (UICSA). *OCEANS 2018 MTS/IEEE Charleston*. 2018.
- [11] Johnson DH, Dudgeon DE. *Array Signal Processing: Concepts and Techniques*. Upper Saddle River NJ: PTR Prentice Hall; 2002.
- [12] Hoorntje RT, Kassam SA. The unifying role of the coarray in aperture synthesis for coherent and incoherent imaging. *Proceedings of the IEEE*. 1990;78(4):735–752.

- [13] BouDaher E, Ahmad F, Amin MG. Sparse reconstruction for direction-of-arrival estimation using multi-frequency co-prime arrays. *EURASIP Journal on Advances in Signal Processing*. 2014;2014(1).
- [14] Zhang YD, Amin MG, Himed B. Sparsity-based DOA estimation using co-prime arrays. 2013 IEEE International Conference on Acoustics, Speech and Signal Processing. 2013.
- [15] BouDaher E, Ahmad F, Amin MG. Sparsity-based extrapolation for direction-of-arrival estimation using co-prime arrays. *Compressive Sensing V: From Diverse Modalities to Big Data Analytics*. 2016.
- [16] Liu C-L, Vaidyanathan PP, Pal P. Coprime coarray interpolation for DOA estimation via nuclear norm minimization. 2016 IEEE International Symposium on Circuits and Systems (ISCAS). 2016.
- [17] Zhou C, Shi Z, Gu Y, Zhang YD. Coarray interpolation-based Coprime Array DOA estimation via covariance matrix reconstruction. 2018 IEEE International Conference on Acoustics, Speech and Signal Processing (ICASSP). 2018.
- [18] Cai TT, Wang L. Orthogonal matching pursuit for sparse signal recovery with noise. *IEEE Transactions on Information Theory*. 2011;57(7):4680–4688.
- [19] Zhou T, Ahmad F, Ouyang B, Li Y. Near-field source localization with an underwater inflatable sonar co-prime array. *Big Data: Learning, Analytics, and Applications*. 2019.
- [20] Dmochowski JP, Benesty J. Steered beamforming approaches for acoustic source localization. *Springer Topics in Signal Processing*. 2010;:307–337.
- [21] Kozick RJ, Coviello C. Wideband Capon beamforming with pre-steering. 2016 50th Asilomar Conference on Signals, Systems and Computers. 2016.
- [22] Li Y, Su T-C, Ouyang B. Design and deployment analysis of subsea deployable structures. 2017 27th International Ocean and Polar Engineering Conference; 2017.
- [23] Li Y, Stankovic R, Ouyang B, Su T-C. Study on flexural properties of tubular underwater inflated structures filled with hydrogel beads. *Journal of Civil Engineering and Construction*. 2019;8(2):48–54.
- [24] Li Y, Thomas J, Ouyang B, Su T-C, Zhou T, Ahmad F. Design and experimental study of underwater inflatable co-prime sonar array (UICSA). *OCEANS 2019 MTS/IEEE SEATTLE*. 2019.
- [25] Hydrofoam [Internet]. HMI. [cited 2022Jan24]. Available from: <https://hmicompany.com/concrete-raising/polyurethane-foam-materials/hydrofoam/>
- [26] RESON TC 4013 – HYDROPHONE [Internet]. ProductPage. [cited 2022Jan24]. Available from: <http://www.teledynemarine.com/reson-tc4013?ProductLineID=48>
- [27] Aquarian Audio Products H2A-XLR hydrophone user's guide [Internet]. [cited 2022Jan24]. Available from: [https://www.aquarianaudio.com/AqAudDocs/H2a\\_XLR\\_manual.pdf](https://www.aquarianaudio.com/AqAudDocs/H2a_XLR_manual.pdf)
- [28] Orcaflex Help [Internet]. WebHelp. [cited 2022Jan24]. Available from: <https://www.orcina.com/webhelp/OrcaFlex/Default.htm>
- [29] Li Y, Thomas J, Ouyang B, Su T-C, Ahmad F. Numerical study of underwater inflatable Co-Prime Sonar Array (UICSA). Volume 4: Pipelines, Risers, and Subsea Systems. 2020.
- [30] INSMY portable IPX7 waterproof bluetooth speaker, wireless outdoor SPE [Internet]. INSMY. [cited 2022Jan24]. Available from: <https://insmy.net/products/insmy-portable-ipx7-waterproof-bluetooth-speaker-wireless-outdoor-speaker-shower-speaker-with-hd-sound-support-tf-card-suction-cup-12h-playtime-for-kayaking-boating-hiking-teal>
- [31] Zoom. H6 audio recorder [Internet]. ZOOM. [cited 2022Jan24]. Available from: <https://www.zoom-na.com/products/field-video-recording/field-recording/zoom-h6-handy-recorder-1#specs>
- [32] Liu C-L, Vaidyanathan PP. Robustness of difference coarrays of sparse arrays to sensor failures—part I: A theory motivated by Coarray Music. *IEEE Transactions on Signal Processing*. 2019;67(12):3213–3226.



© 2022 by the author(s). This work is licensed under a [Creative Commons Attribution 4.0 International License](http://creativecommons.org/licenses/by/4.0/) (<http://creativecommons.org/licenses/by/4.0/>). Authors retain copyright of their work, with first publication rights granted to Tech Reviews Ltd.